APPLICATION OF ARTIFICIAL INTELLIGENCE METHODS IN FLATFOOT ASSESSMENT

Birutė Sinkutė[1] , Justina Šeštokė[1*, 2], Eglė Butkevičiūtė[3]
[1] St. Ignatius Loyola College, Kaunas, Lithuania
[2]Prof. K. Barsauskas Ultrasound Research Institute, Kaunas University of Technology, Lithuania
[3]Department of Software Engineering, Faculty of Informatics, Kaunas University of Technology, Lithuania
[*]Corresponding author: justina.sestoke@ilk.lt

ABSTRACT
This study examined the potential of artificial intelligence tools for detecting flatfoot pathology. We want to emphasise that there is very little research in this area and to point out that this is a relevant and very important topic in medicine. First, the base flow used a pre-trained "backbone" on the ImageNet dataset. In this study, this term refers to the feature extraction part of a convolutional network. A standardised pre-processing with pruning and augmentation was performed, and a three-stage training schedule (stages 1, 2, and 3), average and maximum aggregation at the subject level, and the addition of light test time were proposed. Nine different model architectures were used. From stage 2 onwards, all models were trained on feet. Three-dimensional photographs with real flatfoot shapes, from flatfoot stages I to IV, were used. The most validated model was displayed in accurate AUROC plots, with estimated average and maximum aggregation values and their standard deviations. The research and calculations demonstrate the feasibility of applying artificial intelligence in orthopaedics. This work aimed to apply artificial intelligence methods and to detect flat feet.

Keywords: *orthopaedics; flat feet; artificial intelligence; 2D images.*

1. INTRODUCTION
Flat feet are a common problem among patients visiting musculoskeletal clinics. This condition, often called *pes planus*, *planovalgus* foot, or fallen arches, can be congenital or acquired. There are many causes of acquired flatfoot, including posterior tibial tendon degeneration, trauma, neuroarthropathy, neuromuscular disease and inflammatory arthritis. Of these, tibial tendon degeneration is probably the most common. The foot is distinguished from other parts of the body by its contact with the ground during movement, which is why its structure and function are so important. Each bone connects to another, forming a closed movement system through which each movement disorder can reach other parts of the system: the knee, hip joints, back, and neck **[1–3]**. The foot is unique in that it is in contact with the ground during movement, which is why its structure and function are so important. Each bone connects to the others, forming a closed movement system through which any movement disorder can reach other parts of the system: the knees, hips, back, and neck [2–4].
Anatomically, it is accepted that the foot consists of three parts: the ankle, which allows the shin bones to connect to the foot, the midfoot, and the toes. The main function of the ankle and foot is to absorb shock and generate force when walking. The sole absorbs most of the load on the body, but if the foot does not perform its function properly, other parts of the body (knees, hips, spine, etc.) receive increased load, which can eventually lead to damage to the musculoskeletal system [5–7]. At first glance, the foot may seem like a simple part of the body that requires little attention, but when we examine it anatomically, we see that it is a complex assembly

of bones, muscles, ligaments, and joints. In flatfoot, the arches of the feet descend downward, and the foot itself turns inward. Flatfoot is influenced by weakness of the ligaments and muscles, so the correct shape of the arches is not maintained. If the arches do not form, the entire posture of a person is disrupted [6–9].
This work aimed to apply artificial intelligence methods and to detect flat feet.
Recently, various artificial intelligence tools have been widely used in almost all fields. The field we are considering is no exception. A publication attempts to determine whether a pathology is present in a camera image [10]. The article examines lateral images of the foot; such images are not widely used in orthopaedics. In our publication, we present a scan of the foot from below. By applying various artificial intelligence tools, we will determine the presence/absence of flatfoot.
The paper is organised as follows. Section 1 reviews foot function and pathology, and presents the theoretical background. The application of artificial intelligence tools for pathology detection is reported in Section 2. The conclusions and discussion are in Section 3.

2. FOOT FUNCTION AND PATHOLOGY

To apply AI tools correctly, it is first necessary to understand the foot's function and anatomy. Therefore, this chapter introduces the anatomy and pathology of the foot.
Foot Function. The foot has two arches: the longitudinal and the transverse. The foot has three arches and is presented in Figure 1 **[2,11,12]**:

- The lateral longitudinal arch, which is the arch on the outer side of the foot. This arch is responsible for supporting the foot, and the force of the body's weight is transmitted through it from the lower leg.
- The medial longitudinal arch, which is the arch found along the inner part of the foot, is characterised by soft tissues and interarticular cartilage. The purpose of the medial longitudinal arch is to cushion contact with the ground.
- The transverse arch of the foot is located across the foot, connecting the first and fifth metatarsals.

Figure 1. The foot arches.

The calcaneus is a common bone of both the outer and inner arches. The inner arch consists of the calcaneus, the talus (through which the foot connects to the arch), the navicular bone, three arches and the I–III metatarsals. The outer arch consists of the calcaneus, cuboid bone, the IV and V metatarsals. Ligaments and muscles influence the shape of the arches. The arches of the feet fluctuate with load. On the inner side,

5-7 cm, and on the outer side, about 2 cm. The most significant part in maintaining the shape of the arches is the lintel stone, located at the top of the arch and connecting the arcuate bridge or arcuate gate structure. The foot has one scutellum in each arch. These scutella are the scutellum, the talus and the inner scutellum. The base of the foot consists of three main support points—the base of the calcaneus, the head of the I metatarsal with two sesamoid bones, and the head of the V metatarsal. In a healthy foot, all three points distribute the load and connect into a triangle with the help of arches (Figure 2) [13-15].

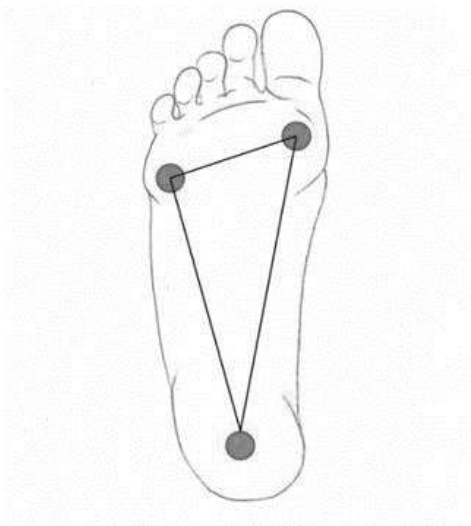

Figure 2. Foot base.

The base of the foot (3 support points) is extremely important for the body's balance and posture. If the muscles' work is disrupted, this alters the biomechanics of walking, and the support points can shift, leading to irregular posture, coordination problems, and joint and bone deformities.

Acquired flat feet were classified according to the Johnson and Strom system, which ranges from I to III, in 1997. Merson added a fourth grade. The grading system helps clinicians assess the severity of AAFD and can guide treatment plans. Stage I is characterised by tenosynovitis of the posterior tibial tendon without arch collapse. Patients with stage II adult-acquired flatfoot have collapsed feet and are unable to perform a single-leg heel raise. This stage is further divided into stages IIa and IIb. Stage IIa has a foot drop with a valgus deformity of the hindfoot but no midfoot abduction, while stage IIb has midfoot abduction. Patients with stage III adult-acquired flatfoot have a fixed deformity with valgus deformity of the hindfoot and abduction of the forefoot. Patients with stage IV deformity have ankle valgus due to weakening of the deltoid ligament **[16–20]**:

Stage I. Stage I is the mildest form of PTT dysfunction. Patients may have a history of tenosynovitis or tendinosis with mild to moderate pain along the tendon course. The hindfoot is mobile and normally flexed. The PTT can still invert and lock the hindfoot during heel-lift, allowing the patient to stand on the toes. Radiographs may be normal, although MRI may show PTT inflammation or early signs of degeneration.

Stage II. In stage II, deformity and impaired function develop. However, the deformity remains flexible, and passive correction can be achieved by adducting and inverting the metatarsophalangeal joint. As the PTT degenerates and lengthens, the foot inverts less actively, and the transverse metatarsal joints can no longer be locked, and the toes can no longer be supported. Later, the bones distal to the talus rotate

laterally, and the talocrural joint subluxes, resulting in hindfoot valgus and forefoot abduction. The unsupported talus is now plantarflexed. At some point, the spring ligament may weaken, contributing to increased deformity. A stage IIA deformity is characterised by minimal abduction at the midfoot and less than 30% tarsal coverage on a standing AP radiograph. A stage IIB deformity is still flexible, but there is greater forefoot abduction (>30% tarsal coverage). The distinction between stages IIA and IIB may help determine the treatment approach.

Stage III. Stage III represents a more fixed deformity, where correction by passive inversion to neutral is no longer possible. The hindfoot is in a fixed valgus position, while the forefoot is abducted.

Stage IV. A stage IV deformity differs from the other stages in that the ankle joint is involved. In stage IV, the deltoid ligament is insufficient, resulting in lateral talar tilt and valgus deformity of the tibia. Although some patients have tibial deformity and flexible flatfoot (stage IVa), most have rigid foot deformities due to damage to the ankle joint (stage IVb). In addition to tibial deformity, ankle joint arthritis may be present. Uncorrectable flatfoot is characterised by impaired foot support, gait changes, discomfort when standing or walking, rapid fatigue in the foot area, and coordination changes.

This assessment scale is suitable for evaluating foot posture in adults. The assessment scale is used to assess the position of the foot (pronation-supination) and to determine whether the foot is supinated, neutral, or pronated (flatter). This is not a direct diagnosis of “flatfoot”, but a very good tool for assessing foot posture and monitoring changes. Other methods:

- Clinical examination (assessment of arch height, heel axis, gait);
- Standing on tiptoes (if the flexible arch is restored—this is physiological flatfoot);
- Photopodometry or plantography;
- Jack test (restoration of the arch of the foot by lifting the toe);
- X-ray - only if additional diagnostics are needed.

Orthopaedic care involves selecting orthopaedic devices. Their range is extremely wide, including half- and full-foot inserts, footwear, and insoles, but they are ineffective if the flatfoot stage is misdiagnosed. Therefore, after reviewing all the main features of the anatomy and pathology of the foot, we can use artificial intelligence tools and determine the presence/absence of pathology.

3. APPLICATION OF ARTIFICIAL INTELLIGENCE (AI) TOOLS FOR PATHOLOGY DETECTION

This investigation presents a methodology based on the application of artificial intelligence tools to identify flatfoot pathology. Using the Elinvision iQube scanner, 2D images were obtained to reflect the patient’s foot structure. The scanner accuracy 0.5 mm, scanning area (L × W × H) 40 × 180 × 150 mm ± 5 mm; scan time is 5–9 s; file format—png; heel positioning laser Integrated heel positioning laser allows to align patient’s foot/ankle for the better scan result; 3D texture in colour allows to view and evaluate the condition of the sole and markings made by physicians; calibrated 2D texture in color provides more accurate data in images. The dataset comprised 42 paediatric subjects, each contributing two plantar images (left and right foot), for a total of 84 images. Clinical labels were provided at the subject level and mapped to both feet: 33 subjects were classified as healthy and 9 subjects as flatfoot (see Table 1). Only binary labels (healthy vs flatfoot) were available; no gradation of flatfoot severity (e.g., stages I–III) was provided. Labels were assigned by an orthopaedist as

healthy vs flatfoot. Those classified as having flexible flatfoot according to routine clinical assessment were labelled as ‘flatfoot’. Asymptomatic individuals with a normal medial longitudinal arch and neutral hindfoot alignment were labelled as ‘non-flatfoot’. All “flatfoot” cases (regardless of suspected stage) were merged into one positive class. For this study, a binary label (flatfoot vs non-flatfoot) was used.

Stages were not modelled separately due to the small sample size. Written consent to participate in the study was obtained from all subjects. The study was conducted in accordance with the ethical principles of the Declaration of Helsinki (64th WMA General Assembly, Fortaleza, Brazil, October 2013). Identifiable information was removed from the collected data to ensure subject anonymity. An example of the images used is shown in Figure 3. Standardisation and sorting of scanned data (e.g., consistent foot positioning, illumination) were performed to ensure data uniformity and reliability. Analysis of existing databases and diagnostic tools for 3D image processing and classification, e.g., specialised 3D CNN architectures or hybrid models that combine 3D geometric analysis with 2D feature extraction.

Table 1. Dataset summary

	Number of Subjects	Number of Images
Controls (no flatfoot)	33	66
Flatfoot	9	18
Total	42	84

Figure 3. Left and right patient feet.

In this study (see Figure 4), the term backbone refers to the feature-extraction part of a convolutional network. The backbone receives an image and produces a compact representation, after which a single-logit classification head is applied for the binary task. All backbones were initialised with ImageNet pre-trained weights and trained under the same three-stage schedule: the head was trained first (Stage-1), selected late backbone blocks were unfrozen and fine-tuned (Stage-2), and an optional short fine-tune with class-balanced sampling was performed (Stage-3). Multiple backbones were evaluated to characterise differences in architectural bias, capacity, and computational cost under identical data, preprocessing, and optimisation settings.

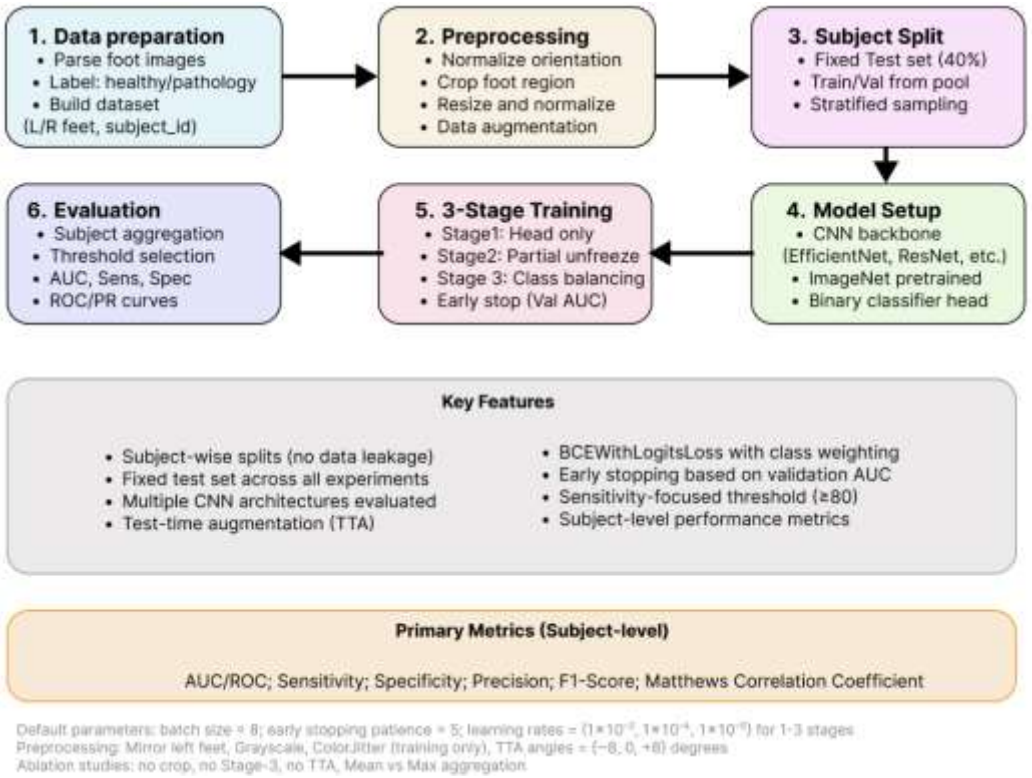

Figure 4. Workflow of the proposed framework for the flat feet classifier.

Nine architectures were assessed. ResNet-50 was used as a strong residual-network baseline whose stability under transfer learning has been widely observed [21]. Dense-Net-121 was included to represent densely connected feature reuse, which is known to be parameter-efficient [22]. EfficientNet-B0 was chosen for its compound scaling and Mobile Inverted Bottleneck (MBConv) blocks, which frequently yield favourable accuracy-to-compute trade-offs on small datasets [23]. Two lightweight families: MobileNetV2 and MobileNetV3 (Small and Large) were included to reflect mobile/edge deployment constraints while retaining competitive transfer performance [24,25]. ConvNeXt-Tiny was used as a modern convolutional design that replaces some batch-norm/activation patterns with LayerNorm and larger effective kernels, offering transformer-like training behaviour while remaining fully convolutional [26]. Two very efficient baselines, ShuffleNetV2 (×1.0) and SqueezeNet1.1, were added to probe the lower end of the parameter/FLOP spectrum [27,28]. All backbones were used only as feature extractors. The final classification layer was replaced with a single fully connected unit producing a single logit.

A fixed subject-held-out test set was created once and kept unchanged for all experiments. The test set contained 40% of subjects (patient-wise split; exact counts are reported in the Dataset section). The remaining subjects formed a training/validation pool. For each backbone, models were trained in 20 independent repeats: in each repeat, a new stratified subject split was drawn from the pool to form a small validation set used for early stopping and threshold selection. Results were reported on the same fixed test set, and summary values were given as mean ± standard deviation across repeats.

Performance was computed at the subject level. Image scores for the same subject (e.g., left/right feet) were first aggregated into a single subject score using either the mean or max aggregation method, as specified. A decision threshold was then chosen

for the validation subjects to achieve≥80% sensitivity. When that target was not reachable, the Youden index (maximising TPR–FPR) was used. Sensitivity was defined as the proportion of pathology subjects correctly flagged as positive. Specificity was defined as the proportion of healthy subjects correctly flagged as negative. “Subject accuracy” refers to the fraction of test subjects correctly classified after aggregation and thresholding. The baseline pipeline was used: ImageNet-pretrained backbone, standardised pre-processing with cropping and padding, the proposed three-stage training schedule (head-only → partial unfreeze → class-imbalance fine-tune), mean or max aggregation at the subject level, and light test-time augmentation. Under the proposed baseline pipeline, subject-level performance was stable across backbones when mean aggregation was used (Figure 5). Across repeats, variability is shown as mean (± std), and no additional confidence intervals are reported to avoid over-interpretation on a small test cohort. The top models achieved the highest average AUROC with modest variability across repeats, while lower-capacity models trailed by a consistent margin. This pattern indicates that the pre-processing and 3-stage schedule transfer well across architectures, with differences largely attributable to backbone capacity.

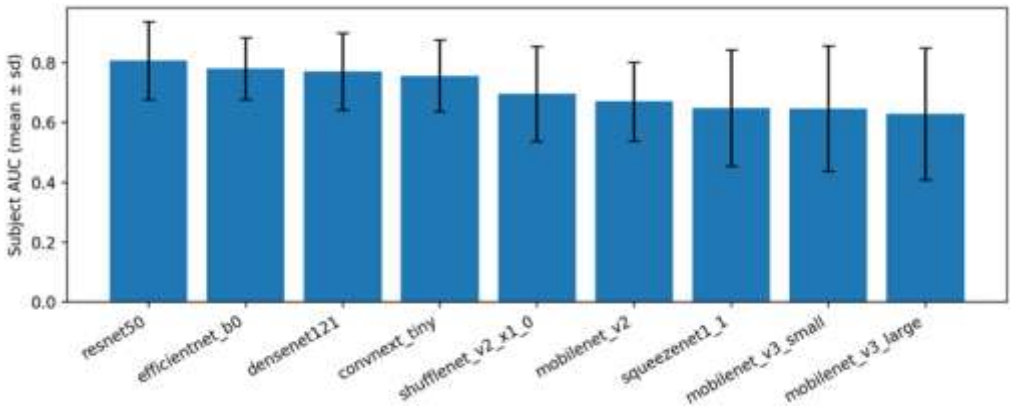

(a)

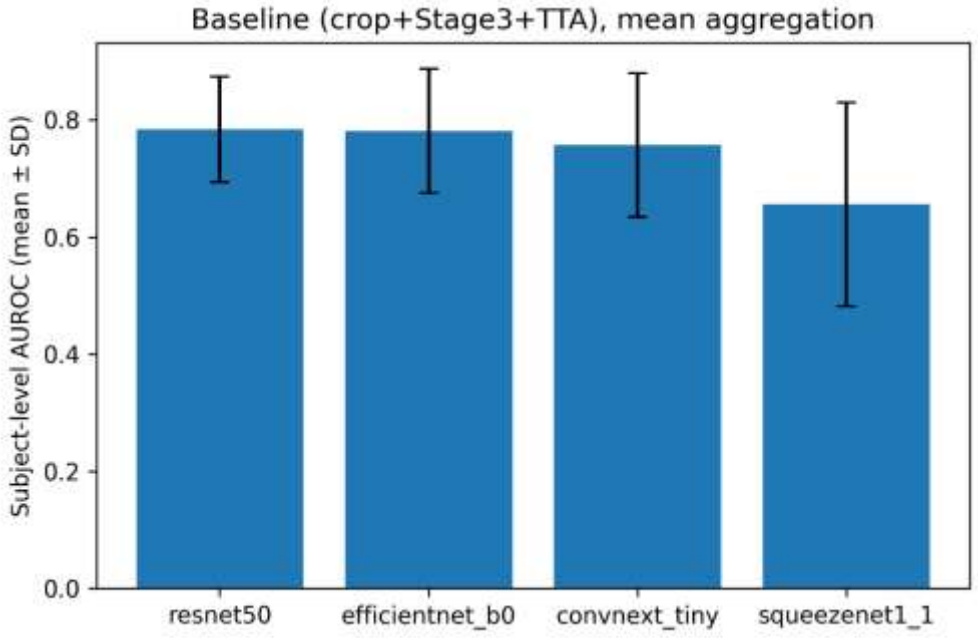

(b)

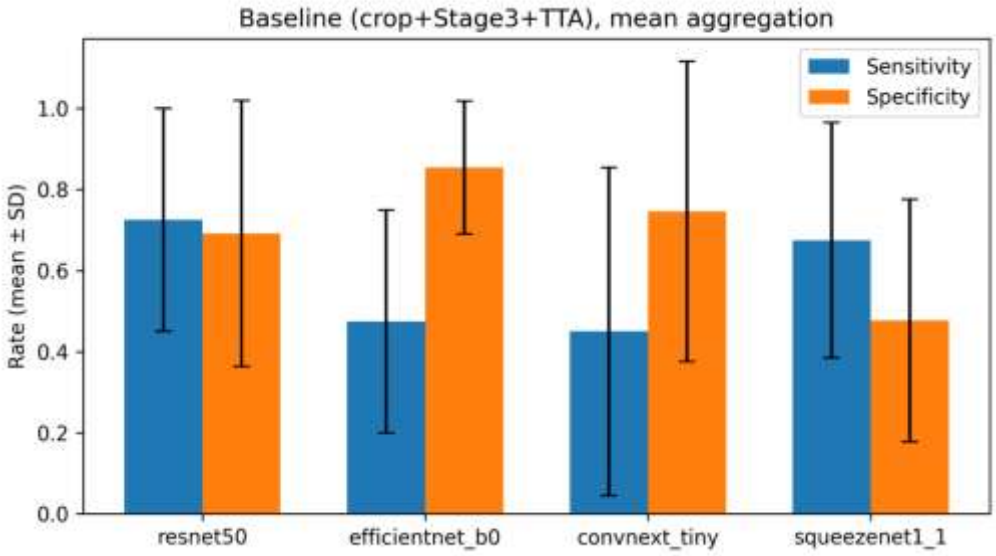

(c)

Figure 5. Baseline subject-level AUROC with mean aggregation.

Under the baseline configuration (cropping, Stage-3, and test-time augmentation) with mean aggregation, subject-level AUROC ranged from ~0.66 to ~0.78 across the four backbones evaluated (Figure 5b). The two strongest performers were ResNet-50 (AUROC 0.784 ± 0.090) and EfficientNet-B0 (0.781 ± 0.106), while ConvNeXt-Tiny was close (0.757 ± 0.123) and SqueezeNet1.1 trailed (0.656 ± 0.174). Sensitivity–specificity trade-offs differed by model (Figure 5c): EfficientNet-B0 favoured specificity on this dataset (0.854 ± 0.164) at the cost of lower sensitivity (0.475 ± 0.275), whereas ResNet-50 yielded more balanced behaviour (sens 0.725 ± 0.275; spec 0.692 ± 0.328). Aggregate confusion matrices directly visualise these patterns (e.g., EfficientNet-B0 shows fewer false positives but more false negatives than ResNet-50). All results are subject-level and were computed under strictly subject-wise splits to avoid leakage. The present study was conducted on a small sample (84 images from 42 subjects), a major limitation for both statistical power and model generalisation. The reported results should therefore be interpreted as exploratory rather than definitive. In particular, the model was not explicitly stratified or adjusted for age, sex, BMI, or foot size, and it cannot be assumed that the learned decision boundary is stable across these factors. Uncertainty is expressed as the standard deviation across repeated subject-wise splits. Formal confidence intervals and hypothesis tests were not reported due to the limited cohort size, to avoid over-interpretation. The small cohort makes the results sensitive to differences in age, body mass, and foot morphology. With few subjects, a model can learn patterns that reflect this case mix rather than general features of flatfoot. No stratification or adjustment by age, BMI, or foot size was performed, and no normalisation for these factors was applied. Therefore, the reported metrics should be read as conditional on this cohort.

4. CONCLUSIONS

This study presents a methodology based on the application of artificial intelligence tools to detect flatfoot pathology. 2D images were measured to reflect the patient's foot structure. The observations showed that the proposed three-stage training system, together with orientation normalisation, cropping and dilation preprocessing, and test-

time padding, is the main source of reliability. The specific backbone mainly modulates the absolute performance level. Using 9 different models and training them 20 times, after applying the proposed model improvements, it is possible to assess the presence/absence of flatfoot pathology.

Regarding subject aggregation, the maximum aggregation often yielded a slightly higher AUROC, but the average aggregation was generally more stable across repetitions and produced a more balanced sensitivity and specificity profile. Our study and the proposed methodologies showed the best accuracy with two architectures—resnet50 and efficientnet_b0, which have accuracies of 0.808 (±0.13) and 0.781 (±0.103) when the average aggregation value is used, and 0.861 (±0.118) and 0.855 (±0.12) when the maximum aggregation value at the study level is used. In the future, we plan to apply this method to determine the stages of flatfoot pathology described in this article. This is a new and complex process, but in orthopaedics, it would help determine the stage of pathology more quickly and accurately.

REFERENCES

1. Holowka, N.B.; Wallace, I.J.; Lieberman, D.E. Foot strength and stiffness are related to footwear use in a comparison of minimally- vs conventionally-shod populations. Sci. Rep. 2018, 8, 3679. https://doi.org/10.1038/s41598-018-21916-7.
2. Kostkevičius, G.; Astromskas, R.A. Visos Bėdos Dėl Pėdos; Verslo Respublika: Kaunas, Lithuania, 2010, ISBN: 978-609-95180-0-8.
3. Lo, W.-T.; Wong, D.P.; Yick, K.-L.; Ng, S.P.; Yip, J. The biomechanical effects and perceived comfort of textile-fabricated insoles during straight-line walking. Prosthet. Orthot. Int. 2018, 42, 153–162. https://doi.org/10.1177/0309364617696084.
4. Martinelli, N.; Bianchi, A.; Prandoni, L.; Maiorano, E.; Sansone, V. Quality of Life in Young Adults after Flatfoot Surgery: A Case-Control Study. J. Clin. Med. 2021, 10, 451. https://doi.org/10.3390/jcm10030451.
5. Mohd Shariff, S.; Manaharan, T.; Ahmad Shariff, A.; Merican, A.F. Evaluation of Foot Arch in Adult Women: Comparison between Five Different Footprint Parameters. Sains Malays. 2017, 46, 1839–1848. https://doi.org/10.17576/jsm-2017-4610-22.
6. Nagano, H.; Begg, R. Shoe-Insole Technology for Injury Prevention in Walking. Sensors 2018, 18, 1468. https://doi.org/10.3390/s18051468.
7. Pasapula, C.; Cutts, S. Modern Theory of the Development of Adult Acquired Flat Foot and an Updated Spring Ligament Classification System. Clin. Res. Foot Ankle 2017, 5, 247. https://doi.org/10.4172/2329-910X.1000247.
8. Shi, Q.Q.; Li, P.L.; Yick, K.-L.; Li, N.-W.; Jiao, J. Effects of contoured insoles with different materials on plantar pressure offloading in diabetic elderly during gait. Sci. Rep. 2022, 12, 15395. https://doi.org/10.1038/s41598-022-19814-0.
9. Su, S.; Mo, Z.; Guo, J.; Fan, Y. The Effect of Arch Height and Material Hardness of Personalized Insole on Correction and Tissues of Flatfoot. J. Healthc. Eng. 2017, 2017, 8614341. https://doi.org/10.1155/2017/8614341.
10. Ghandour, S.; Lebedev, A.; Tung, W.-S.; Semianov, K.; Semjanow, A.; DiGiovanni, C.W.; Ashkani-Esfahani, S.; Pineda, L.B. Utilization of artificial intelligence in the diagnosis of pes planus and pes cavus with a smartphone camera. World J. Orthop. 2024, 15, 1146–1154. https://doi.org/10.5312/wjo.v15.i12.1146. PMID: 39744730.

11. Subramaniam, S.; Majumder, S.; Faisal, A.I.; Deen, M.J. Insole-Based Systems for Health Monitoring: Current Solutions and Research Challenges. Sensors 2022, 22, 438. https://doi.org/10.3390/s22020438.
12. Takabayashi, T.; Edama, M.; Inai, T.; Kubo, M. Differences in rearfoot, midfoot, and forefoot kinematics of normal foot and flatfoot during running. J. Orthop. Res. 2021, 39, 565–571. https://doi.org/10.1002/jor.24877.
13. Henry, J.K.; Shakked, R.; Ellis, S.J. Adult-Acquired Flatfoot Deformity. Foot Ankle Orthop. 2019, 4, 2473011418820847. https://doi.org/10.1177/2473011418820847.
14. Uhl, J.-F.; Lo Vuolo, M.; Gillot, C. Anatomy of foot and ankle perforator veins. Phlebolymphology 2017, 24, 105–112.
15. Wang, Y.; Li, Z.; Wong, D.W.-C.; Cheng, C.-K.; Zhang, M. Finite element analysis of biomechanical effects of total ankle arthroplasty on the foot. J. Orthop. Transl. 2018, 12, 55–65. https://doi.org/10.1016/j.jot.2017.12.003.
16. Baumfeld, D.; Baumfeld, T.; da Rocha, R.L.; Macedo, B.; Raduan, F.; Zambelli, R.; Alves Silva, T.A.; Nery, C. Reliability of Baropodometry on the Evaluation of Plantar Load Distribution: A Transversal Study. BioMed Res. Int. 2017, 2017, 5925137. https://doi.org/10.1155/2017/5925137.
17. Bresnahan, P.J.; Juanto, M.A. Pediatric Flatfeet—A Disease Entity That Demands Greater Attention and Treatment. Front. Pediatr. 2020, 8, 19. https://doi.org/10.3389/fped.2020.00019.
18. Cen, X.; Gao, L.; Yang, M.; Liang, M.; Bíró, I.; Gu, Y. Arch-Support Induced Changes in Foot-Ankle Coordination in Young Males with Flatfoot during Unplanned Gait Termination. J. Clin. Med. 2021, 10, 5539. https://doi.org/10.3390/jcm10235539.
19. DeSilva, J.; McNutt, E.; Benoit, J.; Zipfel, B. One small step: A review of Plio-Pleistocene hominin foot evolution. Am. J. Phys. Anthropol. 2019, 168, 63–140. https://doi.org/10.1002/ajpa.23750.
20. Flores, D.V.; Mejía Gómez, C.; Fernández Hernando, M.; Davis, M.A.; Pathria, M.N. Adult Acquired Flatfoot Deformity: Anatomy, Biomechanics, Staging, and Imaging Findings. RadioGraphics 2019, 39, 1437–1460. https://doi.org/10.1148/rg.2019190046.
21. He, K.; Zhang, X.; Ren, S.; Sun, J. Deep Residual Learning for Image Recognition. CVPR 2016, https://doi.org/10.48550/arXiv.1512.03385.
22. Huang, G.; Liu, Z.; Van Der Maaten, L.; Weinberger, K.Q. Densely Connected Convolutional Networks. In Proceedings of the 2017 IEEE Conference on Computer Vision and Pattern Recognition (CVPR), Honolulu, HI, USA, 21–26 July 2017. https://doi.org/10.1109/CVPR.2017.243.
23. Tan, M.; Le, Q. EfficientNet: Rethinking Model Scaling for Convolutional Neural Networks. ICML (PMLR) 2019, https://doi.org/10.48550/arXiv.1905.11946.
24. Sandler, M.; Howard, A.; Zhu, M.; Zhmoginov, A.; Chen, L.-C. MobileNetV2: Inverted Residuals and Linear Bottlenecks. In Proceedings of the 2018 IEEE/CVF Conference on Computer Vision and Pattern Recognition CVPR, Salt Lake City, UT, USA, 18–23 June 2018. https://doi.org/10.1109/CVPR.2018.00474.
25. Howard, A.; Sandler, M.; Chen, B.; Wang, W.; Chen, L.-C.; Tan, M.; Chu, G.; Vasudevan, V.; Zhu, Y.; Pang, R.; et al. Searching for MobileNetV3. In Proceedings of the 2019 IEEE/CVF International Conference on Computer

Vision (ICCV), Seoul, Republic of Korea, 27 October–2 November 2019. https://doi.org/10.1109/ICCV.2019.00140.
26. Liu, Z.; Mao, H.; Wu, C.-Y.; Feichtenhofer, C.; Darrell, T.; Xie, S. A ConvNet for the 2020s (ConvNeXt). CVPR 2022, https://doi.org/10.48550/arXiv.2201.03545.
27. Ma, N.; Zhang, X.; Zheng, H.-T.; Sun, J. ShuffleNet V2: Practical Guidelines for Efficient CNN Architecture Design. ECCV 2018, https://doi.org/10.48550/arXiv.1807.11164.
28. Iandola, F.N.; Han, S.; Moskewicz, M.W.; Ashraf, K.; Dally, W.J.; Keutzer, K. SqueezeNet: AlexNet-level accuracy with 50× fewer parameters and <0.5MB model size. arXiv 2016, https://doi.org/10.48550/arXiv.1602.07360.